Proinflammatory Effects of Pyrogenic and Precipitated Amorphous Silica Nanoparticles in Innate Immunity Cells

OXFORD UNIVERSITY PRESS | Toxicological Sciences

Pro-inflammatory effects of pyrogenic and precipitated amorphous silica nanoparticles in innate immunity cells

Journal:	*Toxicological Sciences*
Manuscript ID	TOXSCI-15-0531.R1
Manuscript Type:	Research Article
Date Submitted by the Author:	n/a
Complete List of Authors:	Di Cristo, Luisana; University of Parma, Department of Clinical and Experimental Medicine Movia, Dania; Trinity College Dublin, School of Medicine; Trinity College Dublin, Amber Centre (CRANN Institute) Bianchi, Massimiliano; University of Parma, Department of Clinical and Experimental Medicine Allegri, Manfredi; University of Parma, Department of Biomedical, Biotechnological and Translational Sciences Mohamed, Bashir; Trinity College Dublin, School of Medicine Bell, Alan; Trinity College Dublin, Advanced Microscopy Laboratory Moore, Caroline; Trinity College Dublin, School of Medicine Pinelli, Silvana; University of Parma, Department of Clinical and Experimental Medicine Rasmussen, Kirsten; Joint Research Centre, Institute for Health and Consumer Protection Riego-Sintes, Juan; Joint Research Centre, Institute for Health and Consumer Protection Prina-Mello, Adriele; Trinity College Dublin, School of Medicine; Trinity College Dublin, Amber Centre (CRANN Institute) Bussolati, Ovidio; University of Parma, Department of Biomedical, Biotechnological and Translational Sciences Bergamaschi, Enrico; University of Parma, Department of Clinical and Experimental Medicine
Key Words:	nanoparticles < Agents, macrophage < Immunotoxicology, inflammation < Immunotoxicology
Society of Toxicology Specialty Section Subject Area:	Nanotoxicology [121]

Pro-inflammatory effects of pyrogenic and precipitated amorphous silica nanoparticles in innate immunity cells

Luisana Di Cristo,[*‡] Dania Movia,[‡¶] Massimiliano G. Bianchi,[*] Manfredi Allegri,[†] Bashir M. Mohamed[‡], Alan P. Bell,[§] Caroline Moore,[‡] Silvana Pinelli,[*] Kirsten Rasmussen,[&] Juan Riego-Sintes,[&] Adriele Prina-Mello,[‡¶] Ovidio Bussolati,[†,1] Enrico Bergamaschi[*,2]

[*]*Department of Clinical and Experimental Medicine, University of Parma, Italy;* [†]*Department of Biomedical, Biotechnological and Translational Sciences, University of Parma, Italy;* [‡]*School of Medicine and* [¶]*AMBER centre (CRANN Institute), Trinity College Dublin, Ireland;* [§]*Advanced Microscopy Laboratory, Trinity College Dublin, Ireland;* [&]*Joint Research Centre, Institute for Health and Consumer Protection, Ispra, Italy*

[1]To whom correspondence should be addressed at Department of Biomedical, Biotechnological and Translational Sciences, University of Parma,
Via Volturno 39, Parma, 43125, Italy.
Fax: +39 0521033742. E-mail: ovidio.bussolati@unipr.it

[2]To whom correspondence should be addressed at Department of Clinical and Experimental Medicine, University of Parma,
Via A. Gramsci n° 14, Parma, 43126, Italy.
Fax: +39 0521033099. E-mail: enrico.bergamaschi@unipr.it

ABSTRACT

Amorphous Silica NanoParticles (ASNP) can be synthetized via several processes, two of which are the thermal route (to yield pyrogenic silica) and the wet route from a solution containing silicate salts (to obtain precipitated, colloidal, mesoporous silica or silica gel). Both methods of synthesis lead to ASNP that are applied as food additive (E551). Current food regulation does not require that production methods of additives are indicated on the product label, and, thus, the ASNP are listed without mentioning the production method. Recent results indicate, however, that pyrogenic ASNP are more cytotoxic than ASNP synthetized through the wet route. The present study was aimed at clarifying if two representative preparations of ASNP, NM-203 (pyrogenic) and NM-200 (precipitated), of comparable size, specific surface area, surface charge and hydrodynamic radius in complete growth medium, had different effects on two murine macrophage cell lines (MH-S and RAW264.7 cells). Our results show that, when incubated in protein-rich fluids, NM-203 adsorbed on their surface more proteins than NM-200 and, once incubated with macrophages, elicited a greater oxidative stress, assessed from *Hmox1* induction and ROS production. Flow cytometry and helium ion microscopy indicated that pyrogenic NM-203 interacted with macrophages more strongly than the precipitated NM-200 and triggered a more evident inflammatory response, evaluated with *Nos2* induction, NO production, and the secretion of TNF-α, IL-6 and IL-1β. Moreover, both ASNP synergized macrophage activation by bacterial lipopolysaccharide (LPS), with a higher effect observed for NM-203. In conclusion, the results presented here demonstrate that, compared to precipitated, pyrogenic ASNP exhibit enhanced interaction with serum proteins and cell membrane, and cause a larger oxidative stress and stronger pro-inflammatory effects in macrophages. Therefore, these two nanomaterials should not be considered biologically equivalent.

Keywords: amorphous silica nanoparticles; food additive; inflammation; macrophages; oxidative stress; protein corona

INTRODUCTION

Amorphous Silica NanoParticles (ASNP) are integrated in a wide variety of commercial products for human use, such as pharmaceutical products, paints, cosmetics and food. ASNP can be synthetized through two main methods, the high-temperature thermal route, to yield *pyrogenic silica,* or low-temperature wet routes to form *precipitated*, *colloidal*, *mesoporous* silica or *silica gel* (Napierska *et al.,* 2010). ASNP are produced in tonnage quantities and are, therefore, among the most abundant synthetic nanoparticles currently available on the market. In the last decades, ASNP produced by either thermal or wet methods are used in food, for example as an anti-caking agent for food products in powder form, to remove yeast and protein from beer, as an anti-foaming agent for wine and as a viscosity control for pastes (e.g. ketchup) and other food. ASNP are indicated on the label of the food as the food additive E551 without specification of the production process of the nanomaterial.

The potential toxicity of ASNP has been extensively investigated in several studies (please refer to (Napierska *et al.,* 2010) for a comprehensive review), and experimental evidence of a dose-dependent oxidative stress, cytotoxicity and inflammatory effects has been reported (Athinarayanan *et al.,* 2014; Lin *et al.,* 2006; Morishige *et al.,* 2010; Park and Park 2009). Given that the production process strongly influences surface reactivity (Napierska *et al.,* 2010), several studies take into account its possible implications for the toxicological behaviour of ASNP. For instance, Zhang et al. (Zhang *et al.,* 2012) found that the lung toxicity of pyrogenic ASNP was comparable to or even exceeding that of crystalline silica nanoparticles, known since many years to be highly toxic (Fubini and Hubbard 2003). Moreover, relatively high doses of pyrogenic ASNP resulted in rat liver fibrosis after 84 days of exposure (van der Zande *et al.,* 2014). However, also ASNP produced with wet methods have been found to be endowed with some toxicity (Kaewamatawong *et al.,* 2005; Morishige *et al.,* 2010; Nishimori *et al.,* 2009). As far as precipitated ASNP are concerned, they have been found to produce only transient and reversible neutrophilic lung inflammatory responses at 24 h (Sayes *et al.,* 2007). In addition, precipitated ASNP seem nearly inert when assayed for hemolytic activity (Pavan *et al.,* 2013) and failed to induce significant increases in the frequency of micronucleated binucleate cells (MNBCs) in human lymphocyte populations (Tavares *et al.,* 2014).

However, only a few studies directly compare the toxicity of pyrogenic and precipitated ASNP. An inhalation toxicity study in Wistar rats (Arts *et al.,* 2007) demonstrated that pyrogenic silica induced a more pronounced increase in the expression of lung inflammation markers and, although equally cleared from the tissue, produced more severe histopathological changes than the precipitated form. The structural determinants for this different biological reactivity have been recently investigated using an *in vitro* model (Guichard *et al.,* 2015). The results presented in that study suggested that

the cytotoxicity and genotoxic properties of ASNP are related more to the primary particles size or to the agglomeration than to the production process. On the contrary, other studies attributed the increased cytotoxicity and pro-inflammatory activating effects of pyrogenic ASNP to their higher surface reactivity (Gazzano *et al.,* 2012; Sandberg *et al.,* 2012) or fused chainlike morphology (Zhang *et al.,* 2012). Since pyrogenic and precipitated ASNP of different size and specific surface area were used in these contributions, the question is open if these physico-chemical characteristics contributed to the dissimilar toxicological behavior of the ASNP tested. For instance, due to these different physico-chemical characteristics, the expression of the biological activities of pyrogenic or precipitated ASNP per mass unit or per surface unit led either to consistent (Gazzano *et al.,* 2012) or contrasting conclusions on their relative toxicity ranking (Sandberg *et al.,* 2012).

To address this issue, here we compare the ability of two representative manufactured nanomaterials of comparable size and specific surface area to exert toxic effects and to induce cell activation in two murine macrophage cell lines.

MATERIALS AND METHODS

Reagents. FBS and culture media were purchased from Euro-Clone SpA, Pero, Milan, Italy. CM-H_2DCF-DA was purchased from Molecular Probes, Invitrogen, (Milan, Italy). Sigma-Aldrich (Milan, Italy) was the source of LPS (from *E. coli*, O55:B5 serotype) and of all the other chemicals, whenever not specified otherwise.

Amorphous Silica NanoParticles (ASNP). ASNP samples (NM-200 and NM-203) were obtained from the JRC Nanomaterials Repository hosting representative industrial nanomaterials (Ispra, Varese, Italy). These materials are classified as representative test materials (RTM) and include a (random) sample from one industrial production batch. They are used within the scope of the EU FP7 project "Managing risks of nanomaterials (MARINA)".
NM-200 are precipitated silica produced by wet route, in which a solution of alkali metal silicate is acidified to produce a gelatinous precipitate that is washed and then dehydrated to produce colourless microporous silica particles (Rasmussen *et al.,* 2013). NM-203 are pyrogenic silica produced via the thermal route, that is burning $SiCl_4$ in an oxygen-rich hydrocarbon flame to produce a fume of SiO_2 (Rasmussen *et al.,* 2013).

Transmission Electron Microscopy (TEM). ASNP were dispersed into 0.05 wt% BSA in water, at the concentration of 2.56 mg/mL. The TEM specimens of suspended ASNP were prepared on 300-mesh Cu lacey carbon grids by drop-casting and were visualized under a Jeol 2100 Transmission Electron Microscope (Jeol Ltd., Tokyo, Japan) operating at 200 kV with a Lanthanum Hexaborise emission source.

Nanoparticle Tracking Analysis (NTA). The average hydrodynamic radius of NM-200 and NM-203 in complex dispersion media was characterised using Nanoparticle Tracking Analysis (NTA) developed by Malvern Instruments Limited (Wiltshire, UK). This technique utilises the properties of light scattering and Brownian motion to obtain particle size distributions of samples in liquid suspension (Hole *et al.,* 2013). A NS500 instrument, equipped with a 405 nm laser in conjunction with software version NTA 3.1, was used for the purpose of this study. NM-200 and NM-203 were dispersed in 0.05% BSA-water and sonicated for 15 min with a Branson 5510 sonication bath prior to incubation in the various media, i.e. water, non-supplemented RPMI1640 medium (Gibco, Life Technologies, cat no. 61870) and RPMI medium supplemented with 10% foetal bovine serum (FBS) at three different concentrations (16, 32 and 64 μg/ml). Hydrodynamic radius was measured

after incubation at 37 °C for 0 and 24 h. A nanoparticles concentration that records a minimum of 200 tracks per video was undertaken to obtain statistical significance. Five by 60 s videos were recorded for each sample. Results are reported as average mode ± standard deviation.

Protein adsorption to ASNP. ASNP were incubated for 1 h at 37 °C in RPMI culture medium with 10% FBS. At the end of the incubation, the suspension was centrifuged for 15 min at 13,000*g*, and the pellets were washed three times in 18 mΩ water. Proteins adsorbed to the ASNP were then quantified with a modified micro Lowry protein assay (Farinha *et al.,* 2004) or separated on a 12% (w/v) SDS-PAGE gel. For PAGE, pellets were suspended in Laemmli buffer 1x (250 mM Tris–HCl, pH 6.8, 8% SDS, 40% glycerol, and 0.4M DTT), warmed at 95 °C for 10 min, and aliquots of 25 µl were loaded on gel. The gel was then washed three times in 18 mΩ water and stained through silver staining (Cosmo Bio Co., Ltd., Tokyo, Japan, Cat. No. 423413) according to manufacturer's instructions. The intensity of the protein bands was determined with a Personal Densitometer SI Molecular Dynamics (GE Healthcare Europe GmbH, Milano, Italy) after further staining with Bio-Safe™ Coomassie G-250 Stain (Cat. 161-0786, Bio-Rad Laboratories S.r.l., Milan, Italy) to increase band intensity.

Cell culture. Murine alveolar macrophages (MH-S), a gift of Prof. Dario Ghigo, University of Torino (Italy), were originally provided by the Cell Bank of the Istituto Zooprofilattico Sperimentale della Lombardia ed Emilia-Romagna (Brescia, Italy). RAW264.7 murine peritoneal macrophages were obtained from the Cell Bank of the Istituto Zooprofilattico Sperimentale della Lombardia ed Emilia-Romagna (Brescia, Italy). Cells were routinely cultured in a humidified atmosphere of 5% CO_2 in air in Falcon 10-cm diameter dishes (BD, Bioscience, USA) or in T75 cell culture flasks (Nunc, Fisher Scientific, Ireland) in RPMI1640 medium supplemented with 10% FBS, streptomycin (100 µg/ml) - penicillin (100 U/ml), L-glutamine (2 mM) and (for MH-S cells only) β-mercaptoethanol (0.05 mM). For experiments, cells were seeded in complete growth medium in Falcon 24-well plates (BD Bioscience, San Jose, CA, USA) or Millicell EZ 4-well glass slides (Millipore, Ireland) at a density of 20 x 10^4 cells/well.

Incubation with ASNP and dosimetry. Before the experiments, ASNP were heated at 230 °C for 4 h to eliminate possible contamination from lipopolysaccharide (LPS). After cooling at room temperature, nanomaterials were dispersed in a stock solution at a concentration of 2.5 mg/mL by pre-wetting powder in 0.5% ethanol (96% purity) followed by dispersion in 0.05 wt% Bovine Serum Albumin (BSA, A9418, Sigma Aldrich) in water and 16 min of bath sonication (from

Nanogenotox protocol, with modifications). The ASNP suspensions thus obtained were diluted in complete growth medium to reach the desired dose.

Taking into account the volume/surface ratio of the various culture systems adopted and the use of sub-confluent (for cytotoxicity experiments) or confluent monolayers (for other studies), we have expressed the ASNP nominal doses as μg of materials per cm^2 of monolayer. The volume/culture surface ratio has been kept constant in all the experiments. The dosimetry of nanomaterials, expressed as μg/ml or m^2/ml, is summarized in Table 1.

High content screening and analysis (HCSA) – ASNP cytotoxicity. MH-S and RAW264.7 cells were exposed to increasing doses (2.5, 5, 10, 20, 40, 80 μg/cm^2) of ASNP for 24, 48 and 72 h. Data are reported as average standard deviation ($n_{replicates}$ = 3; n_{tests} = 3). Positive (cells exposed to cisplatin) and negative (untreated cells) controls were also included into each experiment in order to quantify the extent of toxicity response induced by each particle type. After, respectively, 24, 48 and 72 h of incubation, cells were washed in phosphate-buffered saline solution (PBS) at pH 7.4 and fixed in 3% paraformaldehyde (PFA), as previously described (Mohamed *et al.,* 2011; Movia *et al.,* 2011; Movia *et al.,* 2010; Prina-Mello *et al.,* 2013; Williams *et al.,* 2008). Multiparametric analysis of the ASNP cytotoxicity response using HCSA was performed using the Cellomics® HCS reagents Cytotoxicity1 kit and Apoptosis1 kit (Thermo Fisher Scientific, Ireland) according to manufacturer's instructions. The kits allow detecting and quantifying changes in i) cell count, lysosomal mass/pH, cell membrane permeability (as parameters recorded with the Cytotoxicity1 kit) and, ii) mitochondrial activity, cytoskeletal actin reorganisation, nuclear intensity and nuclear size (as parameters recorded with the Apoptosis1 kit), which are phenomena associated to a toxicological response. Plates were analysed by IN Cell Analyzer 1000 automated microscope (GE Healthcare, Buckinghamshire, UK). Cytotoxicity and apoptosis responses were quantified using the analysis module of the IN Cell Investigator software (GE Healthcare, Buckinghamshire, UK). The module allows simultaneous quantification of subcellular inclusions that are marked by different fluorescent probes and measures fluorescence intensity associated with predefined nuclear and cytoplasmic compartments, as previously described (Prina-Mello *et al.,* 2014).

Cellular internalization of ASNP. RAW264.7 cells were plated in 4-well Millicell™ EZ Slide (Merck SpA, Vimodrone, MI, Italy) at a concentration of 20×10^4 cells/well. Cells were incubated for 24 h at 37^0C (5% CO_2) to allow cell attachment to the glass substrate. For internalization, cells were incubated with ASNP at a concentration of 5 μg/cm^2. After 2 h, cells were transferred for 20 min into serum-free medium supplemented with CellTracker™ Red CMPTX (8 μM, Molecular

Probes, Invitrogen) to label the cytoplasm; in the last 10 min 1,5-bis[2-(di-methylamino)ethyl]amino-4, 8-dihydroxyanthracene-9,10-dione (DRAQ5®, 20 μM, Alexis Biochemicals, San Diego, CA, USA) was also added to the incubation medium to counterstain the nucleus. At the end of the incubation, cell monolayers were rinsed in PBS and fixed with 3.7% PFA at room temperature for 15 min. Specimens were then mounted on glass slides with fluorescence mounting medium (Dako Italia SpA, Milan, Italy) and imaged by confocal microscopy. Confocal analysis was carried out with a LSM 510 Meta scan head integrated with an inverted microscope (Carl Zeiss, Jena, Germany). Samples were observed through a 40× (1.4 NA) oil objective. Image acquisition was carried out in multitrack mode, i.e. through consecutive and independent optical pathways. Excitation at 488 nm and reflectance were used to visualize ASNP (shown in green as pseudo-colour); excitation at 543 nm and emission recorded through a 580–630 nm band pass barrier filter were used to visualize the cytoplasm (red, pseudo-colour); excitation at 633 nm and emission through a 670 nm long pass filter were recorded to visualize the nucleus (blue, pseudo-colour).

Cytofluorimetric assay of ASNP uptake. The light scattered at a 90° angle to the axis of the laser beam is measured as side scatter (SSC) and is related to intracellular density, a parameter associated with ASNP uptake (Zhao and Ibuki 2015)**.** For these experiments, RAW264.7 cells were seeded in 6-well plates at the density of 1 x 10^6 cells/well. After 30 min or 2 h of incubation with NM-200 or NM-203 (5 μg/cm^2), cells were washed with PBS, detached with a cell scraper and analysed by a FC500™ flow cytometer (Beckman Coulter, Brea, CA, USA), as previously described (Alinovi *et al.,* 2015) The cytograms and the histogram were obtained using FlowJo software (Ashland, OR, USA).

He-Ion Microscopy (HIM). Cells were fixed at room temperature in 2.5% glutaraldehyde in 0.1 M Sørensen's phosphate buffer (pH 7.3) and rinsed with Sørensen's phosphate buffer. Samples were dehydrated in increasing concentrations of EtOH (from 70% up to 100%). The final wash was carried out in pure EtOH for 20 min. The samples were air dried and imaged by a Zeiss Orion Plus He-ion microscope (Carl Zeiss, Oberkochen, Germany) using an accelerating voltage of 30 kV. Samples were transferred into the chamber, which had undergone plasma clean overnight prior to loading samples, using a load lock. The working distance was 8 mm and a 10 μm beam limiting aperture was used. The probe current was between 0.5 and 1.5 pA. Images were acquired by collecting the secondary electrons emitted by the interaction between the He-ion beam and the

specimen with an Everhart-Thornley detector (part of the He-ion microscope system). The image signal was acquired in a 32- or 64-line integration to each contributing line of the image.

Gene expression analysis. The expression of *Nos2*, *Hmox1* and *Tnf* was assessed with real Time PCR. 1 µg of total RNA, isolated with GenElute Mammalian Total RNA Miniprep Kit (Sigma–Aldrich) was reverse transcribed. For real-time qPCR, cDNA was amplified with Go Taq PCR Master Mix (Promega, Italia, Milan, Italy), along with the forward and reverse primers indicated in Table 2 (5 pmol each). The expression of the gene of interest under each experimental condition was normalized to that of *Gapdh* and shown relative to its expression level in control, untreated cells.

Cell lysis and Western blotting. Cells were lysed in a buffer containing 20 mM Tris–HCl, pH 7.5, 150 mM NaCl, 1 mM EDTA, 1 mM EGTA, 1% Triton, 2.5 mM sodium pyrophosphate, 1 mM β-glycerophosphate, 1 mM Na_3VO_4, 1 mM NaF, 2 mM imidazole and a cocktail of protease inhibitors (Complete, Mini, EDTA-free, Roche, Milan, Italy). Lysates were sonicated for 15 s and centrifuged at 12,000g for 20 min at 4 °C. After quantification with the Bio-Rad protein assay, aliquots of 40 µg of proteins were mixed with Laemmli buffer 4× (250 mM Tris–HCl, pH 6.8, 8% SDS, 40% glycerol, and 0.4M DTT), warmed at 95 °C for 10 min and loaded on a 8% gel for SDS-PAGE. After electrophoresis, proteins were transferred to PVDF membranes (Immobilon-P, Millipore, Millipore Corporation, MA, USA). Non-specific binding sites were blocked with an incubation of 1 h at room temperature in 5% BSA in TBS-Tween. The blots were then exposed at 4 °C overnight to anti-Nos2 (rabbit polyclonal, 1:400, Santa Cruz Biotechnology) or anti-actin (rabbit polyclonal, 1:30,000, Cell Signaling Technology diluted in the same solution). After washing, the blots were exposed for 1 h at room temperature to HRP-conjugated anti-rabbit antibody (Cell Signaling Technology), diluted 1:20,000 in blocking solution. Immunoreactivity was visualized with Immobilon Western Chemiluminescent HRP Substrate (Millipore, Milan, Italy).

Determination of NO production. Nitrite concentration in the culture media, as an indicator of NO production, was determined through a fluorometric approach, as previously described (Sala *et al.,* 2002). The method is based on the production of the fluorescent molecule 1H-naphthotriazole from 2,3-diaminonaphthalene (DAN) in acid environment. For nitrite determination, 100 µl of medium were put in wells of a black 96-well plate with a clear bottom (Corning, Cambridge, MA, USA). DAN (20 µl of a solution of 0.025 mg/ml in 0.31 M HCl) was then added and, after 10 min at room temperature, the reaction was stopped with 20 µl of 0.7 N NaOH. Standards were performed in the

same medium from a solution of 1 mM sodium nitrite. Fluorescence was determined with an EnSpire plate reader (Perkin Elmer). Nitrite production was expressed in nmoles per ml of extracellular medium (μM).

Cytokine secretion. After the selected incubation periods in presence of ASNP, the presence of Tumor Necrosis Factor-alpha (TNF-α), Interleukin-6 (IL-6) and IL-1β in the culture media of the MH-S and RAW264.7 was determined with ELISA RayBio® kits (Ray Biotech, Norcross, GA, USA). 100 μl of medium were transferred into 96-well plates functionalized with anti-cytokine antibodies and incubated overnight at 4 °C. Then, 100 μl of biotinylated antiIgG-antibody were added in each well and, after 1 h of incubation at RT, 100 μl of streptavidin solution were added. After 45 min, samples were incubated with 100 μl of the TMB One Step Reagent, contained in the kit solution; after 30 min, reaction was stopped and absorbance was immediately read at 450 nm with a plate reader. Standards were performed in the assay buffer from a solution of 50 ng/ml of the recombinant cytokine, as for manufacturer's protocol.

Intracellular reactive oxygen species production. The production of ROS was measured using 5-(and-6)-chloromethyl-2',7' dichlorodihydrofluorescein diacetate, acetyl ester (CM-H_2DCF-DA, Cat. No. C6827, Molecular Probes, Invitrogen). After the experimental treatments, cells were incubated with the probe (5 μM) for 2 h at 37 °C. Cells were then washed twice with PBS and the fluorescence was determined (485 nm λ_{ex} and 520 nm λ_{em}) with a multiplate reader. Hydrogen peroxide (6 mM, one hour before adding the probe) was used as a positive control. Cell fluorescence was visualized using a fluorescence microscope (Nikon, Tokyo, Japan).

Statistics and data presentation. Statistic evaluation of effects has been performed with two-tail t test for unpaired data to compare positive (LPS in Figs. 4, 5 and 6C-D; H_2O_2 in Fig. 6A-B) and negative controls. One-way ANOVA with Tukey test has been used in all the other cases. Statistical evaluations have been performed using GraphPad Prism™ software version 4.00 (GraphPad Software Inc., San Diego, CA). Differences have been considered significant for values of $p < 0.05$. In order to screen and normalise the results of High Content Screening, KNIME in combination with a screening module HiTS (http://code.google.com/p/hits, 0.3.0) were implemented as previously described (Kozak *et al.,* 2010; Williams *et al.,* 2008). All measured parameters were normalized using the percent of the positive controls. Z score was used for scoring the normalized values. These scores were summarized using the mean function as follows Z score= (x-mean)/StDev, as from previous work (Birmingham *et al.,* 2009; Movia *et al.,* 2011; Movia *et al.,*

2010; Prina-Mello *et al.,* 2013; Williams *et al.,* 2008). Heatmap graphical illustration in a colorimetric gradient table format was adopted as the most suitable schematic representation to report on any statistical significance and variation from normalized controls based on their Z score value. Heatmap tables illustrate the range of variation of each quantified parameter from the minimum (green) through the mean (yellow) to the maximum (red) accordingly to the parameter under analysis.

RESULTS

Physico-chemical properties of ASNP

A detailed physico-chemical characterization of the ASNP, provided in the report on the synthetic amorphous silicon dioxide nanomaterials of the JRC Repository (Rasmussen *et al.,* 2013), is summarized in Table 3.

The TEM images of NM-200 and NM-203 (Fig. S1) indicated that both nanomaterials mainly consist of small aggregates of some elementary particles that tend to clump in larger agglomerates, while primary particles are rarely detected.

Table 4 reports the average hydrodynamic radius of each sample, at the maximal dose used in the biological experiments, in water, non-supplemented medium and protein-supplemented medium, as recorded by NTA. A high standard deviation in the measurements of NM-200 and NM-203 samples dispersed in water and non-supplemented culture medium was associated with a broad range in distribution of nanoparticles sizes and with agglomeration phenomena. ASNP dispersed in medium supplemented with 10% FBS showed a more mono-dispersed population. NM-203 showed a decreasing trend in hydrodynamic radius after 24 h incubation, indicating the breakdown of particle agglomerates. Interestingly, minor changes in the hydrodynamic radius of the two samples dispersed in supplemented medium were recorded over time, suggesting the stabilisation of the nanoparticle dispersion or formation of protein corona by FBS. Under conditions resembling those adopted for the biological experiments (*i.e.* t = 24 h, RPMI supplemented with FBS) the hydrodynamic radius of NM-200 and NM-203 was comparable.

Binding of serum proteins to ASNP

In order to evaluate the binding of serum proteins with ASNP, NM-200 and NM-203 were incubated with culture medium supplemented with 10% FBS. Proteins adsorbed to ASNP were then quantified with a colorimetric method or detected with silver staining after polyacrylamide gel electrophoresis (Fig. 1). Quantification of adsorbed proteins (Fig. 1A) evidenced that ASNP bound serum proteins in a dose-dependent trend, with significantly higher amounts for NM-203 than for NM-200. The increased adsorption capability of NM-203 was confirmed with silver staining (Fig. 1B-C), for either FBS or pure BSA. The adsorbed protein pattern was different for the two ASNP types, with a few bands clearly more abundant in NM-200 than in NM-203 eluate.

Interaction of ASPN with macrophages

MH-S and RAW264.7 cells were imaged by He-Ion Microscopy (HIM) after 24 h incubation with NM-200 and NM-203 (Fig. 2). Untreated cells (negative control) cultured for 24 h were also imaged for comparison (Fig. 2A-B, G-H). Many ASNP agglomerates could be found in close proximity of the exposed cells and, in some cases, cells surface was partially or completely covered by an ASNP layer. In particular, NM-203 (see the representative fields shown in Fig. 2E-F and 2M-N) formed agglomerates onto the cell surface more readily than NM-200 (Fig. 2C-D and 2I-L). Moreover, MH-S cells interacted with NM-200 agglomerates more closely than RAW264.7 cells.

Cell internalization of ASNP

The internalization of ASNP was assessed in RAW264.7 cells after 2 h of incubation with confocal microscopy and cytofluorimetry. Images evidenced that both ASNP (imaged in reflectance mode) were effectively internalized into the macrophages (Fig. S2). In addition, the cytogram distribution, recorded by cytofluorimetry, and the corresponding histograms (Fig. 3), showed an increase in SSC intensity after treatment with both ASNP for 30 min, thus suggesting that ASNP were rapidly taken up by the macrophages. However, the mean SSC ratio was higher for NM-203 than for NM-200 at both 30 min (17%) and 2 h (56%) of treatment, indicating a more efficient uptake of the pyrogenic ASNP.

Cytotoxicity of ASNP on murine macrophages

Recent data from our and other laboratories, obtained with several independent methods on a wide range of NM-200 and NM-203 doses at various incubation times (Farcal *et al.,* 2015), indicated that NM-203 cause a larger decrease in cell viability than NM-200 in both MH-S and RAW264.7 cell models.

Changes in cell count recorded and quantified by HCSA confirmed that NM-203 were more cytotoxic than NM-200 (Fig. S3-S6). Increased apoptotic response was also higher for NM-203 than NM-200-treated cells. Several other parameters also changed with different patterns suggesting that the interaction of the two nanomaterials with macrophages triggered various cytotoxicity and apoptotic pathways, as reported in the supplemental information section.

Macrophage activation by pyrogenic and precipitated ASNP

Fig. 4A reports *Nos2* mRNA expression after 24 h incubation of MH-S macrophages to non-cytotoxic doses (5 or 10 μg/cm^2) of NM-200 or NM-203. *Nos2* was significantly induced by incubation with NM-200 (at 10 μg/cm²) or NM-203 (at both 5 and 10 μg/cm²). This effect was confirmed at protein level (Fig. 4C) and corresponded to a clear cut increase in NO production (Fig.

4E). However, in RAW264.7 cells *Nos2* messenger was not significantly induced compared with control under the same experimental conditions (Fig. 4B), although, only in cells treated with NM-203, Nos2 protein appeared barely detectable and, consistently, increased accumulation of nitrites in the medium was observed (Fig. 4D-F).

Recently, a synergistic effect on macrophage activation has been described for TiO_2 NP and LPS (Bianchi *et al.,* 2015). To assess if also ASNP synergize LPS effects on macrophages, RAW264.7 cells were simultaneously treated with LPS and either ASNP (Fig. 4G). The combined treatment caused a further significant stimulation of NO production, compared with that observed after incubation with LPS alone. The enhancing effect was much higher for NM203-treated (+52%) compared to NM200-treated cells (+18%).

Secretion of pro-inflammatory cytokines in MH-S and RAW264.7 cells exposed to ASNP

The secretion of the pro-inflammatory cytokines TNF-α, IL-6 and IL-1β was quantified in the culture medium after the treatment of MH-S and RAW264.7 cells with NM-200 and NM-203 (5 or 10 μg/cm²). Under control conditions, the levels of the three cytokines in the culture medium were very low or below threshold. However, both cell lines produced a significant increase of medium TNF-α (assessed at 6 h of treatment), IL-6 (at 12 h) and IL-1β (after 48 h of treatment), although MH-S cells consistently secreted more cytokines than RAW264.7 cells. At the higher dose used (10 $\mu g/cm^2$), and with both cell models, pyrogenic ASNP elicited a higher secretion of the three cytokines than precipitated ASNP.

Oxidative stress in ASNP-exposed murine macrophages

ROS production was measured on MH-S and RAW264.7 macrophage lines upon 24 h of incubation with NM-200 and NM-203 (Fig. 6). A significant dose-dependent increase of ROS production was detectable, by fluorescence signal recording, in NM-203-treated MH-S cells (Fig. 6A) but not in NM-203-treated RAW264.7 cells (Fig. 6B). Conversely, NM-200, did not promote ROS production either in MH-S cells or in RAW264.7 cells. The increase in fluorescence in MH-S cells treated with NM-203 was also evident by fluorescence microscopy (Fig. 6).

Hmox-1 (hemeoxygenase-1) is known to play a major role in the cell response to oxidative stress-mediated injuries (Bhaskaran *et al.,* 2012). *Hmox1* expression was assessed after a 6h-incubation with NM-200 and NM-203. For both macrophage lines, a dose-dependent increase in expression of *Hmox1* messenger was evident for NM-203-treated cells, although in MH-S the increase of the messenger was much higher than in RAW264.7 cells (10- and 12-fold for 5 and 10 μg/cm² respectively for MH-S, and 6- and 9-fold induction for 5 and 10 μg/cm² respectively for

RAW264.7) (Fig. 6C-D). In contrast, for both MH-S and RAW264.7 cells, NM-200 induced an increase in expression of the *Hmox1* messenger only at a concentration of 10 µg/cm², with a much lower effect for RAW264.7 cells.

The expression of *Hmox1* and *Tnf* was assessed after 8 h in RAW264.7 cells exposed to 10 µg/cm² of ASNP in the absence or in the presence of the antioxidant N-acetyl-cysteine (NAC, 1 mM). NAC significantly blunted the induction of *Tnf* in macrophages incubated with NM-203, but not with NM-200, although lowered *Hmox1* induction by both materials (from 4-fold to 2-fold for NM-200 and from 11-fold to 5-fold for NM-203, Fig. 6E-F).

DISCUSSION

The results presented in this study indicate that pyrogenic NM-203 ASNP are more biologically reactive than precipitated NM-200 ASNP. In particular, NM-203 resulted more cytotoxic and exhibit larger effects on macrophage activation than NM-200, suggesting that the thermally produced synthetic amorphous silica is correlated to the presence of crucial determinants of biological responses.

The identification of structural determinants of nanomaterial toxicity is greatly aided by the comparison of biological effects of different preparations of the same nanoparticles. However, to derive clear cut conclusions, the comparison should be ideally performed between nanomaterials differing by a single property only. In the present study, this principle has been applied to the evaluation of the biological effects of precipitated and pyrogenic ASNP, differing only in the method of synthesis. The characterization of NM-200 and NM-203, obtained from the JRC Nanomaterials Repository, had indicated comparable values of specific surface area, size of primary particles and agglomerates, and zeta potential (Rasmussen *et al.,* 2013). We have integrated those data, showing that in FBS-supplemented media, *i.e.* under the conditions adopted for biological experiments, NTA measurements did not show significant differences in the hydrodynamic radius between NM-200 and NM-203. Moreover, no significant further agglomeration was detected in this complex dispersing medium over a 24 h incubation. These data suggest that differences detected in the biological responses following cell incubation with NM-200 and NM-203 are not attributable to the different agglomeration of the two materials.

The different production processes lead to different surface chemistries with oxidative reactivity for NM-203 and null or reductive reactivity for NM-200 (Rasmussen *et al.,* 2013). In a protein-rich medium, different surface reactivity could modify the formation of protein corona, which is known to be a powerful determinant of the biological interactions of the nanomaterials (Ge *et al.,* 2015). The adsorption of proteins to ASNP has been previously investigated (Turci *et al.,* 2010) but no comparison was made in that study between pyrogenic and precipitated silica. The direct comparison between the two ASNP performed here (Fig. 1) not only indicated that pyrogenic ASNP bound a larger quantity of serum proteins than precipitated silica but also showed that the pattern of adsorbed proteins was not the same in the two cases. As Turci *et al.* (Turci *et al.,* 2010) reported, the adsorption of a protein on a surface is a very complex process that results from a contribution of energetic (hydrogen bonding, electrostatic forces, and hydrophobic interactions) and entropic factors (structural changes in the protein and dehydration of the protein and surface). In our case, the zeta potential values of the two ASNP were very similar; therefore we can exclude surface

charge as the main reason of different uptake and specificity towards single serum protein. Zhang et al. (Zhang *et al.,* 2012) have argued that, although a wide range of ASNP are endowed with similar coverages of surface silanols, this does not exclude distinct toxicity profiles. The same authors demonstrate that a major determinant of the different toxicity of ASNP produced by thermal or wet routes derives from differences in the siloxane framework architecture, attributable to the synthesis conditions. In that study, the Stober wet method was used for the production of colloidal ASNP. If the hypothesis proposed by Zhang *et al.* would be applicable also for the pyrogenic and precipitated ASNP tested in the present study, we could speculate that specific domains of serum proteins may have a structure that better fits the surface characteristics (i.e. the siloxane framework) of the two ASNP preparations.

Nanoparticle surface may also adsorb organic molecules other than proteins, which may affect the biological interactions of the nanomaterials. For instance, we recently demonstrated that the interaction between TiO_2 NP and LPS strongly potentiates macrophage activation, suggesting that the presence of environmental contaminants may enhance the pro-inflammatory activity of nanomaterials (Bianchi *et al.,* 2015). As far as ASNP are concerned, Shi et al (Shi *et al.,* 2010) reported that LPS and ASNP have synergistic cytotoxic and oxidative effects on A549 lung epithelial cells. Our results demonstrate that ASNP enhanced LPS effects also on macrophage activation, with a much higher effect observed for the pyrogenic NM-203. Several mechanisms may underlie this synergy; the amount of LPS adsorbed may be larger for pyrogenic than for precipitated ASNP or LPS-induced activation may be indirectly favoured by NM-203 effects on macrophages, for instance, through the promotion of a stronger oxidative stress.

The different surface reactivity stemming from different production processes may also influence the different interaction of the two ASNP with the cell surface. Indeed, Pavan et al. reported that the different interaction between various types of amorphous silica (pyrogenic, precipitated, vitreous) and red blood cells (RBC) is mainly determined by the surface arrangement of silanols and siloxanes that are able to match with epitopes present in the RBC membrane (Pavan *et al.,* 2013). The resulting hemolysis, evident for pyrogenic and vitreous but not for precipitated silica, could be correlated with the pathogenic responses to amorphous silica nanoparticles (Pavan *et al.,* 2013) and, at least for vitreous silica, with inflammasome activation (Pavan *et al.,* 2014). In our study, helium ion microscopy (Fig. 2) has been used to investigate the interaction of ASNP with the cell membrane. NM-203, but not NM-200, clearly formed aggregated layers onto the plasma membrane of both macrophage lines, so that the cell surface was completely or partially covered by ASNP. Close interaction with cell membrane of pyrogenic silica and changes in membrane morphology were previously reported by electron microscopy (Zhang *et al.,* 2012). However, no obvious

differences between pyrogenic and precipitated ASNP internalization were found in macrophages with the same technique (Gazzano *et al.,* 2012). In contrast with those results, our cytofluorimetric analysis indicates that, at least at a short time of incubation, NM-203 enter cells more efficiently than NM-200 ASNP (Fig. 3).

All the inflammatory parameters tested (*Nos2* induction at both protein and gene level, NO production, TNF-α, IL-6 and IL-1β secretion) were more evident in NM-203- than in NM-200-treated macrophages. Importantly, although the effects were overall more evident in MH-S cells than in RAW 264.7 cells, the ranking of biological effects was consistently NM-203 > NM-200 in the two macrophage cell lines. Our results are consistent with recent studies that have reported higher cytotoxicity and inflammatory activity of pyrogenic, as compared to precipitated or colloidal ASNP, towards macrophages (Gazzano *et al.,* 2012; Sandberg *et al.,* 2012; Zhang *et al.,* 2012). Although we do not specifically investigate the activation modality elicited by ASNP, all the parameters taken into consideration are consistent with M1 or "classical" macrophage activation, a coordinated response at transcriptional level that plays a major role in promoting acute inflammation. It is known that M1 activation of inflammatory cells is associated with oxidative stress (Park and Park 2009). Thus, the higher cytotoxicity and the greater pro-inflammatory responses induced by NM-203 in both macrophage cell lines may be due to the higher oxidative stress withstood by cells exposed to this material. In support of our hypothesis, we have demonstrated that pyrogenic ASNP are more powerful inducers of *Hmox1* than precipitated ASNP. Given that *Hmox1* induction is one of the most sensitive and reliable indicators of the cell response to oxidative stress and a parameter linked to inflammation triggering (Naito *et al.,* 2014; Poss and Tonegawa 1997), these results indicate that NM-203-treated cells undergo a higher level of oxidative stress than NM-200-treated cells, a conclusion also supported by the results of the CM-H_2DCF fluorescence test (Fig. 6). The role of oxidative stress in the response to ASNP is also supported by the effects of the antioxidant NAC, which partially hinders, along with *Hmox1* expression, also *Tnf* induction in NM203-treated cells. However, this partial inhibition, along with the NAC insensitivity of the NM-200-dependent stimulation of *Tnf* induction, suggests that ASNP promote cytokine production through a complex mechanism only in part attributable to oxidative stress.

A significant dose-dependent increase in IL-1β secretion was detected in macrophages exposed to ASNP. Such response was particularly evident in NM-203-treated macrophages, and pointed to the activation of the inflammasome, as already reported in previous studies from other research groups. However, those studies were performed on THP-1 cells activated with phorbol esters (Zhang *et al.,* 2012) or on RAW264.7 cells primed by LPS (Sandberg *et al.,* 2012) and exposed to high doses of

pyrogenic ASNP (50-200 μg/ml). Conversely, in our study we demonstrated the activation of inflammasome in non-primed macrophages exposed to relatively low, barely toxic doses of pyrogenic ASNP. Moreover, for the first time, our results also show the activation of this pathway by precipitated ASNP, although with a smaller potency compared with pyrogenic silica. Since maturation of IL-1β is tightly regulated by the NLRP3 inflammasome, our results suggest that even low doses of pyrogenic and precipitated nanoparticles are able to stimulate both *Il1* expression and proIL-1β processing.

In conclusion, the data presented in this study demonstrate that pyrogenic NM-203 are more cytotoxic and pro-inflammatory than precipitated NM-200 of comparable size and surface area. Taking into account also the literature data as outlined above, the greater biological reactivity of pyrogenic ASNP does not seem to depend on a different agglomeration behaviour when dispersed in biological media but may, instead, derive from their higher surface reactivity associated with a higher capability to: i) adsorb proteins and, possibly, other bioactive organic molecules, ii) interact with cell membranes and iii) induce oxidative stress in exposed cells. With this in mind, lowering the particle surface reactivity should be considered as part of the "safety by design" approaches to reduce biological hazard derived from exposure to pyrogenic ASNP. Moreover, as substantiated above, the biological reactivity of pyrogenic and precipitated ASNP should be presumed to be different and, in our opinion, there is thus a need for a labelling that would report the method of synthesis when ASNP are present in food and, possibly, in other products.

SUPPLEMENTARY DATA

TEM micrographs of ASNP, confocal images of internalized ASNP and multiparametric analysis of the ASNP cytotoxicity response using HCS.

ACKNOWLEDGEMENTS

Supported by NANoREG (Grant FP7-NMP2012 310584), MaRiNa (Grant FP7-NMP4-LA-2011-26321) and QNANO TCD-TA136 (Grant INFRA-2010-1.1.31-262163) for financial contribution to this manuscript. The authors declare that they have no competing interests.

REFERENCES

Alinovi, R., Goldoni, M., Pinelli, S., Campanini, M., Aliatis, I., Bersani, D., Lottici, P. P., Iavicoli, S., Petyx, M., Mozzoni, P., and Mutti, A. (2015). Oxidative and pro-inflammatory effects of cobalt and titanium oxide nanoparticles on aortic and venous endothelial cells. *Toxicol In Vitro* **29**, 426-437.

Arts, J. H., Muijser, H., Duistermaat, E., Junker, K., and Kuper, C. F. (2007). Five-day inhalation toxicity study of three types of synthetic amorphous silicas in Wistar rats and post-exposure evaluations for up to 3 months. *Food Chem Toxicol* **45**, 1856-1867.

Athinarayanan, J., Periasamy, V. S., Alsaif, M. A., Al-Warthan, A. A., and Alshatwi, A. A. (2014). Presence of nanosilica (E551) in commercial food products: TNF-mediated oxidative stress and altered cell cycle progression in human lung fibroblast cells. *Cell Biol Toxicol* **30**, 89-100.

Bhaskaran, N., Shukla, S., Kanwal, R., Srivastava, J. K., and Gupta, S. (2012). Induction of heme oxygenase-1 by chamomile protects murine macrophages against oxidative stress. *Life. Sci.* **90**, 1027-1033.

Bianchi, M. G., Allegri, M., Costa, A. L., Blosi, M., Gardini, D., Del Pivo, C., Prina-Mello, A., Di Cristo, L., Bussolati, O., and Bergamaschi, E. (2015). Titanium dioxide nanoparticles enhance macrophage activation by LPS through a TLR4-dependent intracellular pathway. *Toxicol Res* **4**, 385-398.

Birmingham, A., Selfors, L. M., Forster, T., Wrobel, D., Kennedy, C. J., Shanks, E., Santoyo-Lopez, J., Dunican, D. J., Long, A., Kelleher, D., Smith, Q., Beijersbergen, R. L., Ghazal, P., and Shamu, C. E. (2009). Statistical methods for analysis of high-throughput RNA interference screens. *Nat Methods* **6**, 569-575.

Farcal, L., Torres Andon, F., Di Cristo, L., Rotoli, B. M., Bussolati, O., Bergamaschi, E., Mech, A., Hartmann, N. B., Rasmussen, K., Riego-Sintes, J., Ponti, J., Kinsner-Ovaskainen, A., Rossi, F., Oomen, A., Bos, P., Chen, R., Bai, R., Chen, C., Rocks, L., Fulton, N., Ross, B., Hutchison, G., Tran, L., Mues, S., Ossig, R., Schnekenburger, J., Campagnolo, L., Vecchione, L., Pietroiusti, A., and Fadeel, B. (2015). Comprehensive In Vitro Toxicity Testing of a Panel of Representative Oxide Nanomaterials: First Steps towards an Intelligent Testing Strategy. *PLoS One* **10**, e0127174.

Farinha, C. M., Mendes, F., Roxo-Rosa, M., Penque, D., and Amaral, M. D. (2004). A comparison of 14 antibodies for the biochemical detection of the cystic fibrosis transmembrane conductance regulator protein. *Mol Cell Probes* **18**, 235-242.

Fubini, B., and Hubbard, A. (2003). Reactive oxygen species (ROS) and reactive nitrogen species (RNS) generation by silica in inflammation and fibrosis. *Free Radic Biol Med* **34**, 1507-1516.

Gazzano, E., Ghiazza, M., Polimeni, M., Bolis, V., Fenoglio, I., Attanasio, A., Mazzucco, G., Fubini, B., and Ghigo, D. (2012). Physicochemical determinants in the cellular responses to nanostructured amorphous silicas. *Toxicol. Sci.* **128**, 158-170.

Ge, C., Tian, J., Zhao, Y., Chen, C., Zhou, R., and Chai, Z. (2015). Towards understanding of nanoparticle-protein corona. *Arch Toxicol* **89**, 519-539.

Guichard, Y., Fontana, C., Chavinier, E., Terzetti, F., Gate, L., Binet, S., and Darne, C. (2015). Cytotoxic and genotoxic evaluation of different synthetic amorphous silica nanomaterials in the V79 cell line. *Toxicol Ind Health*.

Hole, P., Sillence, K., Hannell, C., Maguire, C. M., Roesslein, M., Suarez, G., Capracotta, S., Magdolenova, Z., Horev-Azaria, L., Dybowska, A., Cooke, L., Haase, A., Contal, S., Mano, S., Vennemann, A., Sauvain, J. J., Staunton, K. C., Anguissola, S., Luch, A., Dusinska, M., Korenstein, R., Gutleb, A. C., Wiemann, M., Prina-Mello, A., Riediker, M., and Wick, P. (2013). Interlaboratory comparison of size measurements on nanoparticles using nanoparticle tracking analysis (NTA). *J Nanopart Res* **15**, 2101.

Kaewamatawong, T., Kawamura, N., Okajima, M., Sawada, M., Morita, T., and Shimada, A. (2005). Acute pulmonary toxicity caused by exposure to colloidal silica: particle size dependent pathological changes in mice. *Toxicol Pathol* **33**, 743-749.

Kozak, K., Bakos, G., Hoff, A., Bennett, E., Dunican, D., Davies, A., Kelleher, D., Long, A., and Csucs, G. (2010). Workflow-based software environment for large-scale biological experiments. *J Biomol Screen* **15**, 892-899.

Lin, W., Huang, Y. W., Zhou, X. D., and Ma, Y. (2006). In vitro toxicity of silica nanoparticles in human lung cancer cells. *Toxicol Appl Pharmacol* **217**, 252-259.

Mohamed, B. M., Verma, N. K., Prina-Mello, A., Williams, Y., Davies, A. M., Bakos, G., Tormey, L., Edwards, C., Hanrahan, J., Salvati, A., Lynch, I., Dawson, K., Kelleher, D., and Volkov, Y. (2011). Activation of stress-related signalling pathway in human cells upon SiO2 nanoparticles exposure as an early indicator of cytotoxicity. *Journal of nanobiotechnology* **9**, 29.

Morishige, T., Yoshioka, Y., Inakura, H., Tanabe, A., Yao, X., Narimatsu, S., Monobe, Y., Imazawa, T., Tsunoda, S., Tsutsumi, Y., Mukai, Y., Okada, N., and Nakagawa, S. (2010). The effect of surface modification of amorphous silica particles on NLRP3 inflammasome mediated IL-1beta production, ROS production and endosomal rupture. *Biomaterials* **31**, 6833-6842.

Morishige, T., Yoshioka, Y., Inakura, H., Tanabe, A., Yao, X., Tsunoda, S., Tsutsumi, Y., Mukai, Y., Okada, N., and Nakagawa, S. (2010). Cytotoxicity of amorphous silica particles against macrophage-like THP-1 cells depends on particle-size and surface properties. *Pharmazie* **65**, 596-599.

Movia, D., Prina-Mello, A., Bazou, D., Volkov, Y., and Giordani, S. (2011). Screening the cytotoxicity of single-walled carbon nanotubes using novel 3D tissue-mimetic models. *ACS nano* **5**, 9278-9290.

Movia, D., Prina-Mello, A., Volkov, Y., and Giordani, S. (2010). Determination of spiropyran cytotoxicity by high content screening and analysis for safe application in bionanosensing. *Chem Res Toxicol* **23**, 1459-1466.

Naito, Y., Takagi, T., and Higashimura, Y. (2014). Heme oxygenase-1 and anti-inflammatory M2 macrophages. *Arch Biochem Biophys* **564**, 83-88.

Napierska, D., Thomassen, L. C., Lison, D., Martens, J. A., and Hoet, P. H. (2010). The nanosilica hazard: another variable entity. *Part Fibre Toxicol* **7**, 39.

Nishimori, H., Kondoh, M., Isoda, K., Tsunoda, S., Tsutsumi, Y., and Yagi, K. (2009). Silica nanoparticles as hepatotoxicants. *Eur J Pharm Biopharm* **72**, 496-501.

Park, E. J., and Park, K. (2009). Oxidative stress and pro-inflammatory responses induced by silica nanoparticles in vivo and in vitro. *Toxicol Lett* **184**, 18-25.

Pavan, C., Rabolli, V., Tomatis, M., Fubini, B., and Lison, D. (2014). Why does the hemolytic activity of silica predict its pro-inflammatory activity? *Part Fibre Toxicol* **11**, 76.

Pavan, C., Tomatis, M., Ghiazza, M., Rabolli, V., Bolis, V., Lison, D., and Fubini, B. (2013). In search of the chemical basis of the hemolytic potential of silicas. *Chemical research in toxicology* **26**, 1188-1198.

Poss, K. D., and Tonegawa, S. (1997). Reduced stress defense in heme oxygenase 1-deficient cells. *Proc Natl Acad Sci U S A* **94**, 10925-10930.

Prina-Mello, A., Crosbie-Staunton, K., Salas, G., Morales, M. D., and Volkov, Y. (2013). Multiparametric Toxicity Evaluation of SPIONs by High Content Screening Technique: Identification of Biocompatible Multifunctional Nanoparticles for Nanomedicine. *Ieee Transactions on Magnetics* **49**, 377-382.

Prina-Mello, A., Mohamed, B. M., Verma, N. K., Jain, N., and Volkov, Y. (2014). Advanced methodologies and techniques for assessing nanomaterial toxicity: from manufacturing to nanomedicine screening. In Nanotoxicology: Progress toward Nanomedicine. (N. A. Monteiro-Riviere and L. C. Tran Eds.), 2nd ed. , pp. 155-176. CRC Press. Boca Raton, FL.

Rasmussen, K., Mech, A., Mast, J., and De Temmerman P-J, W. N., Van Steen F, Pizzolon JC, De Temmerman L, Van Doren E, Jensen KA et al (2013). Synthetic Amorphous Silicon Dioxide (NM-200, NM-201, NM-202, NM-203, NM-204): Characterisation and Physico-Chemical Properties. JRC Repository: NM-series of Representative Manufactured Nanomaterials. *JRC Scientific and Policy Reports*.

Sala, R., Rotoli, B. M., Colla, E., Visigalli, R., Parolari, A., Bussolati, O., Gazzola, G. C., and Dall'Asta, V. (2002). Two-way arginine transport in human endothelial cells: TNF-alpha stimulation is restricted to system y(+). *Am J Physiol Cell Physiol* **282**, C134-143.

Sandberg, W. J., Lag, M., Holme, J. A., Friede, B., Gualtieri, M., Kruszewski, M., Schwarze, P. E., Skuland, T., and Refsnes, M. (2012). Comparison of non-crystalline silica nanoparticles in IL-1beta release from macrophages. *Part Fibre Toxicol* **9**, 32.

Sayes, C. M., Reed, K. L., and Warheit, D. B. (2007). Assessing toxicity of fine and nanoparticles: comparing in vitro measurements to in vivo pulmonary toxicity profiles. *Toxicol Sci* **97**, 163-180.

Shi, Y., Yadav, S., Wang, F., and Wang, H. (2010). Endotoxin promotes adverse effects of amorphous silica nanoparticles on lung epithelial cells in vitro. *J Toxicol Environ Health A* **73**, 748-756.

Tavares, A. M., Louro, H., Antunes, S., Quarre, S., Simar, S., De Temmerman, P. J., Verleysen, E., Mast, J., Jensen, K. A., Norppa, H., Nesslany, F., and Silva, M. J. (2014). Genotoxicity evaluation of nanosized titanium dioxide, synthetic amorphous silica and multi-walled carbon nanotubes in human lymphocytes. *Toxicol In Vitro* **28**, 60-69.

Turci, F., Ghibaudi, E., Colonna, M., Boscolo, B., Fenoglio, I., and Fubini, B. (2010). An integrated approach to the study of the interaction between proteins and nanoparticles. *Langmuir* **26**, 8336-8346.

van der Zande, M., Vandebriel, R. J., Groot, M. J., Kramer, E., Herrera Rivera, Z. E., Rasmussen, K., Ossenkoppele, J. S., Tromp, P., Gremmer, E. R., Peters, R. J., Hendriksen, P. J., Marvin, H. J., Hoogenboom, R. L., Peijnenburg, A. A., and Bouwmeester, H. (2014). Sub-chronic toxicity study in rats orally exposed to nanostructured silica. *Part Fibre Toxicol* **11**, 8.

Williams, Y., Byrne, S., Bashir, M., Davies, A., Whelan, A., Gun'ko, Y., Kelleher, D., and Volkov, Y. (2008). Comparison of three cell fixation methods for high content analysis assays utilizing quantum dots. *J Microsc* **232**, 91-98.

Zhang, H., Dunphy, D. R., Jiang, X., Meng, H., Sun, B., Tarn, D., Xue, M., Wang, X., Lin, S., Ji, Z., Li, R., Garcia, F. L., Yang, J., Kirk, M. L., Xia, T., Zink, J. I., Nel, A., and Brinker, C. J. (2012). Processing pathway dependence of amorphous silica nanoparticle toxicity: colloidal vs pyrolytic. *J Am Chem Soc* **134**, 15790-15804.

Zhao, X., and Ibuki, Y. (2015). Evaluating the toxicity of silver nanoparticles by detecting phosphorylation of histone H3 in combination with flow cytometry side-scattered light. *Environ Sci Technol* **49**, 5003-5012.

LEGENDS TO FIGURES

FIG. 1. Protein adsorption to ASNP. Nanoparticles, dispersed in 0.05 wt% BSA, were incubated at the concentration of 16-32-64 μg/ml for 1 h in culture medium with or without 10% FBS. At the end of the incubation, the suspensions were centrifuged, and adsorbed proteins quantified (A) or separated and stained (B-C), as described in Methods. Panel (C) shows the densitometric quantification of the lanes after silver staining. For (A), data are means ± S.D. of 3 independent determinations. **$p<0.01$ and ***$p<0.001$. The lines shown in (A) are linear regression best fits. For NM-200: $y = 0.180\ x + 0.5$ ($r^2 = 0.9930$); for NM-203: $y = 0.198\ x + 3.11$ ($r^2 = 0.9894$). Slopes are statistically different ($p < 0.001$). For (B) and (C) a representative experiment, performed twice with comparable results, is shown. Abbreviations: ASNP, amorphous silica nanoparticles; BSA, bovine serum albumin; NM, nanomaterials.

FIG. 2. He-Ion Microscopy (HIM) images of MH-S and RAW264.7. Cells, grown for 24 h in complete growth medium, were treated for 24 h with the indicated NM at 10 μg/cm^2 and imaged with He-ion microscopy (see Methods). (A-B) Untreated MH-S, (C-D) NM-200-treated MH-S, (E-F) NM-203-treated MH-S cells, (G-H) untreated RAW264.7, (I-L) NM-200-treated RAW264.7 and (M-N) NM-203-treated RAW264.7. (C-F-I-N) Large ASNP agglomerates were visible, as well as partial or complete coverage of cell surface (as indicated by arrows). Images (B), (D), (F), (H), (L) and (N) are magnifications of images (A), (C), (E), (G), (I) and (M) respectively. Abbreviations: ASNP, amorphous silica nanoparticles; NM, nanomaterials.

FIG. 3. Internalization of ASNP into RAW264.7 cells. Cells, grown for 24 h in complete growth medium, were treated with 5 μg/cm^2 of NM-200 (A-C) and NM-203 (B-D). After 30 min or 2 h of treatment, SSC was analyzed using FC500™ flow cytometer (see Materials and Methods). Histograms of cells treated for 30 min (red) or 2 h (blue), A, B. Representative cytograms at 2 h (C, D). Black dots, control, untreated cells. Abbreviations: SSC, side scatter.

FIG. 4. Effects of NM-200 and NM-203 on *Nos2* expression and NO production in MH-S and RAW264.7 cells. For (A), (B), (C), (D), (E) and (F), cells, MH-S and RAW264.7 cells, grown for 24h in complete growth medium, were treated with 5 or 10 μg/cm^2 of NM-200 and NM-203, or with LPS (100 ng/ml), used as a positive control. (A-B) After 24 h of treatment, mRNA was extracted and the expression of *Nos2* evaluated as described in Materials and Methods. (C-D) The expression of the protein Nos2 was assessed through Western Blot in cultures treated in parallel and

extracted after 48 h of treatment. A representative blot is shown, with actin used for loading control (upper panel). In the lower panel the densitometric analysis of the same blot is shown. The experiment was performed twice with comparable results. (E-F) Nitrite concentration was determined in the culture medium of the cells used for the experiment shown in (C-D). For (G), RAW264.7 were treated with 10 μg/cm^2 of NM-200 or NM-203 in the absence or in the presence of LPS (10 ng/ml). After 48 h of treatment, nitrite concentration was determined in the culture medium. For (A) and (B), data are means ± S.D. of 2 independent determinations, each performed twice. For (E) and (F), data are means of four independent determinations ± S.D. For (G), data are means ± S.D. of 3 independent determinations. *p<0.05, **p<0.01 and ***p<0.001 *vs.* untreated, control cells. #p<0.05 and ##p<0.01 *vs.* 5 μg/cm^2 of NM-200. $$p<0.01 *vs.* 10 μg/cm^2 of NM-200. §§p<0.01 *vs.* 5 μg/cm^2 of NM-203. ££p<0.01 and £££p<0.001 *vs.* LPS. Abbreviations: ASNP, amorphous silica nanoparticles; A.U., arbitrary units; *Gapdh*, Glyceraldehyde 3-phosphate dehydrogenase (gene); LPS, lipopolysaccharide; NM, nanomaterials; Nos2, inducible nitric oxide synthetase; S.D., standard deviation.

FIG. 5. TNF-α, IL-6 and IL-1β secretion in MH-S and RAW264.7 cells. Cells, grown for 24 h in complete growth medium, were treated with 5 or 10 μg/cm^2 of NM-200 or NM-203 or with LPS (100 ng/ml), as a positive control. After 6, 12 or 48 h of treatment, for TNF-α, IL-6 or IL-1β respectively, the indicated cytokines were measured in the extracellular medium, as described under Materials and Methods. (A), (C) and (E): MH-S; (B), (D), and (F): RAW264.7. Data are means of 3 independent determinations ± S.D. **p<0.01 and ***p<0.001 *vs.* untreated, control cells; ##p<0.01 and ###p<0.001 *vs.* 5 μg/cm^2 of NM-200. $p<0.05, $$p<0.01 and $$$p<0.001 *vs.* 10 μg/cm^2 of NM-200. §§p<0.01 and §§§p<0.001 *vs.* 5 μg/cm^2 of NM-203. Abbreviations: IL-1β, interleukin-1beta; IL-6, interleukin-6; LPS, lipopolysaccharide; NM, nanomaterials; S.D., standard deviation; TNF-α, tumor necrosis factor alpha.

FIG. 6. ROS production, *Hmox1* and *Tnf* induction in macrophages. For (A), (B), (C), (D), cells, grown in complete growth medium, were treated with 5 or 10 μg/cm^2 of NM-200 or NM-203 or with H_2O_2 (6 mM), as a positive control. (A) and (B). After 24 h of treatment, MH-S (A) or RAW264.7 cells (B) were incubated for 2 h with CM-H_2DCF-DA (5 μM). Fluorescence was determined as described under Materials and Methods. Data are means ± S.D. of 3 independent determinations, each performed twice, *p<0.05, **p<0.01 and ***p<0.001 *vs.* untreated, control cells; $p<0.05 *vs.* 10 μg/cm^2 of NM-200. Before the determination of cell CM-H_2DCF-DA, images of representative fields were taken in phase contrast or with fluorescence microscope. x100. (C) and

(D). After 6 h of treatment with ASNP or LPS (100 ng/ml, positive control), mRNA was extracted and the expression of *Hmox1* evaluated as described in Materials and Methods. (C), MH-S; (D), RAW264.7. Data are means ± S.D. of 2 independent determinations, each performed twice. *p<0.05, **p<0.01 and ***p<0.001 *vs.* untreated, control cells; #p<0.05 and ###p<0.001 *vs.* 5 μg/cm^2 of NM-200; $$p<0.01 and $$$p<0.001 *vs.* 10 μg/cm^2 of NM-200. (E) and (F), RAW264.7 cells were treated for 8 h with 10 μg/cm^2 of NM-200 or NM-203. As indicated, NAC (1 mM) was added 1 h before the incubation with ASNP and maintained throughout the experiment. At the end of the incubation, mRNA was extracted, and the expression of *Tnf* (E) and *Hmox1* (F) was evaluated as described in Materials and Methods. Data are means ± S.D. of 3 independent determinations. **p<0.01 and ***p<0.001 *vs.* untreated, control cells; ##p<0.01 and ###p<0.001 *vs.* NM-203+NAC; §p<0.05 *vs.* NM-200+NAC. Abbreviations: ASNP, amorphous silica nanoparticles; A.U., arbitrary units; CM-H_2DCF-DA,5-(and-6)-chloromethyl-2',7' dichlorodihydrofluorescein diacetate, acetyl ester; *Hmox1*, Hemeoxygenase 1 (gene); H_2O_2, oxygen peroxyde; LPS, lipopolysaccharide; NAC, N-acetyl-cysteine; NM, nanomaterials; S.D., standard deviation; *Tnf*, tumor necrosis factor-alpha (gene).

Table 1.
Dosimetry of ASNP*

Doses (μg/cm^2)	Doses (μg/ml)	Doses (m^2/ml)	
		NM-200	**NM-203**
5	10	0.00189	0.00204
10	20	0.00378	0.00407

*Conversion of the doses used (5 or 10 μg/cm^2). The m^2/ml doses are calculated using the values of specific surface area of ASNP shown in Table 3.

Table 2.
Primers and temperatures of annealing adopted for RT-PCR experiments

Gene	Protein	Forward primer	Reverse primer	T (°C)	Amplicon size (bp)
Inducible Nitric oxide synthetase (*Nos2*)	Inducible Nitric oxide synthetase (Nos2)	5'-GTT CTC AGC CCA ACA ATA CAA GA-3'	5'-GTG GAC GGG TCG ATG TCA C-3'	57	127
Hemeoxygenase 1 (*Hmox1*)	Hemeoxygenase 1 (HO-1)	5'-AGG TAC ACA TCC AAG CCG AGA-3'	5'-CAT CAC CAG CTT AAA GCC TTC T-3'	57	86
Glyceraldehyde 3-phosphate dehydrogenase (*Gapdh*)	Glyceraldehyde 3-phosphate dehydrogenase (Gapdh)	5'-TGT TCC TAC CCC CAA TGT GT-3'	5'-GGT CCT CAG TGT AGC CCA AG-3'	57	137
Tumor Necrosis Factor (*Tnf*)	Tumor Necrosis factor-alpha (TNF-α)	5'-CCC TCA CAC TCA GAT CAT CTT C-3'	5'-GCT ACG ACG TGG GCT ACA G-3'	55	61

Table 3.
Physico-chemical properties of the ASNP tested*

Nanomaterial	Indicative content of SiO_2 (%wt)[a]	Crystallinity	Primary Particle size (nm)	Specific surface area (m^2/g)	Zeta potential (surface charge)	Redox Potential
NM-200	96 (EDS)	amorphous	14 ± 7 (TEM)	189.16 (BET)	-47.5 (mV) (in milliQ water, at pH 7)	Inactive or reductive (Oxo Dish fluorescence, sensor plate for O_2 detection)
NM-203	99 (EDS)	amorphous	13± 6 (TEM)	203.92 (BET)	-46.1 (mV) (in milliQ water at pH 6.6)	Oxidative Reactivity (Oxo Dish fluorescence, sensor plate for O_2 detection)

*Data are taken from (Rasmussen *et al.,* 2013)
[a] The content of Si is 44.77 and 46.32 (%wt) for NM-200 and NM-203, respectively.

Table 4.
Hydrodynamic radius of NM-200 and NM-203 (at 64 µg/ml) as determined by Nanoparticle Tracking Analysis (NTA)

Water	Mode t:0 h	Mode t:24 h
NM-200	206.8 ± 25.1nm	274.5 ± 87.2nm
NM-203	349.5 ± 43.9nm	170.6 ± 36.7nm
RPMI medium		
NM-200	355.1 ± 96.2nm	323.0 ± 97.3nm
NM-203	304.3 ± 30.7nm	262.3 ± 25.0nm
RPMI medium + 10% FBS		
NM-200	129.1 ± 6.7nm	137.3 ± 11.5nm
NM-203	173.5 ± 14.0nm	138.3 ± 16.4nm

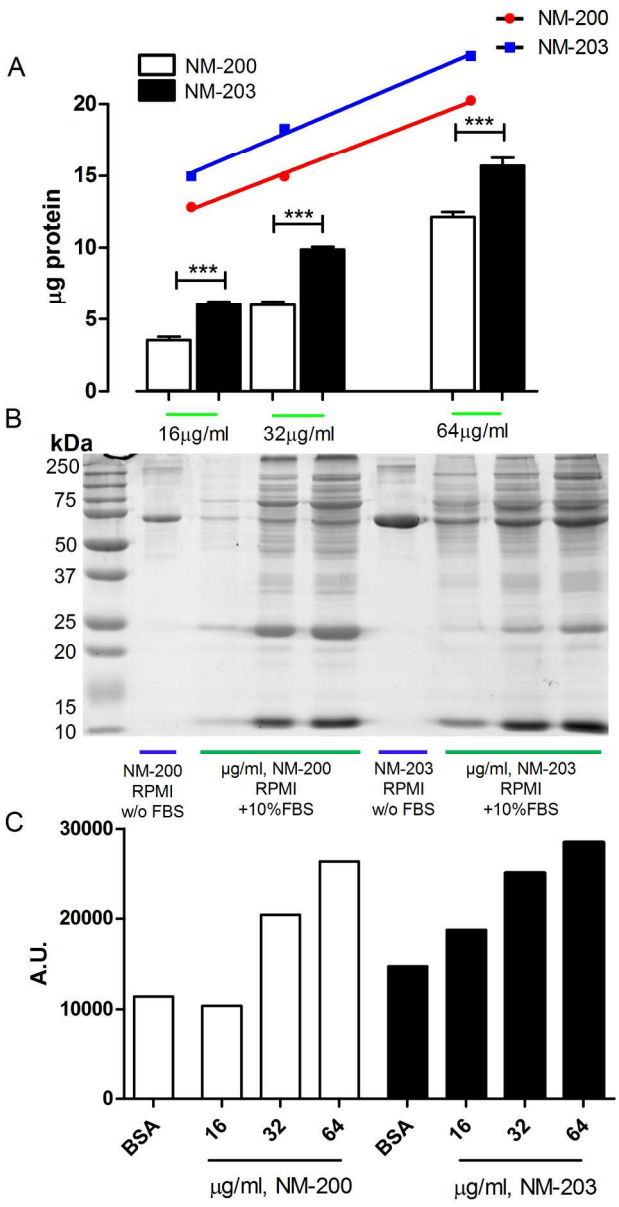

FIG. 1. Protein adsorption to ASNP. Nanoparticles, dispersed in 0.05 wt% BSA, were incubated at the concentration of 16-32-64 μg/ml for 1 h in culture medium with or without 10% FBS. At the end of the incubation, the suspensions were centrifuged, and adsorbed proteins quantified (A) or separated and stained (B-C), as described in Methods. Panel (C) shows the densitometric quantification of the lanes after silver staining. For (A), data are means ± S.D. of 3 independent determinations. **p<0.01 and ***p<0.001. The lines shown in (A) are linear regression best fits. For NM-200: y = 0.180 x + 0.5 (r^2= 0.9930); for NM-203: y = 0.198 x + 3.11 (r^2 = 0.9894). Slopes are statistically different (p< 0.001). For (B) and (C) a representative experiment, performed twice with comparable results, is shown. Abbreviations: ASNP, amorphous silica nanoparticles; BSA, bovine serum albumin; NM, nanomaterials.
150x275mm (300 x 300 DPI)

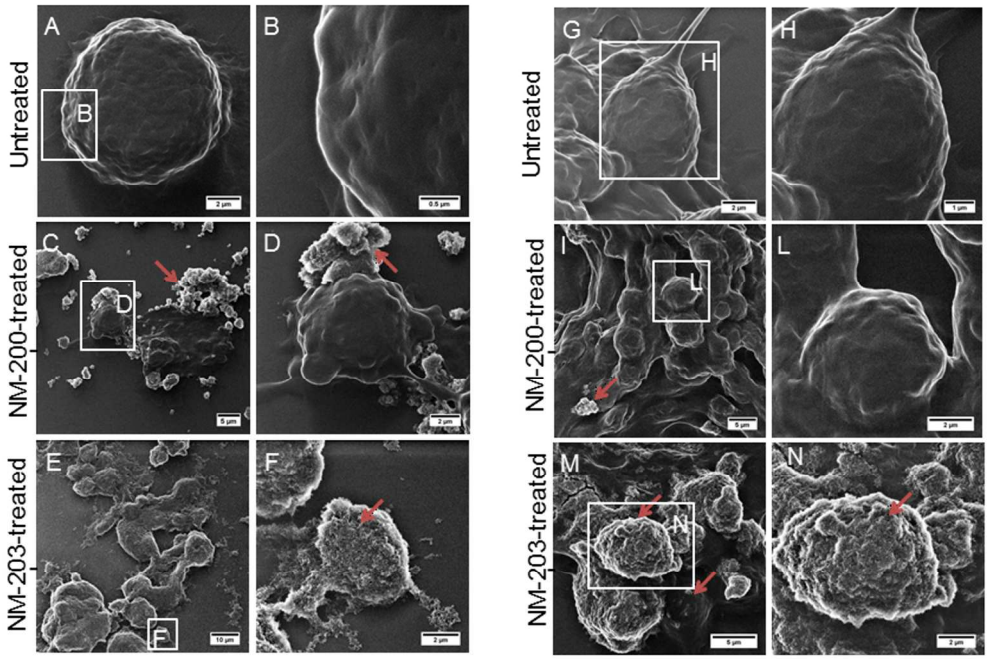

FIG. 2. He-Ion Microscopy (HIM) images of MH-S and RAW264.7. Cells, grown for 24 h in complete growth medium, were treated for 24 h with the indicated NM at 10 μg/cm^2 and imaged with He-ion microscopy (see Methods). (A-B) Untreated MH-S, (C-D) NM-200-treated MH-S, (E-F) NM-203-treated MH-S cells, (G-H) untreated RAW264.7, (I-L) NM-200-treated RAW264.7 and (M-N) NM-203-treated RAW264.7. (C-F-I-N) Large ASNP agglomerates were visible, as well as partial or complete coverage of cell surface (as indicated by arrows). Images (B), (D), (F), (H), (L) and (N) are magnifications of images (A), (C), (E), (G), (I) and (M) respectively. Abbreviations: ASNP, amorphous silica nanoparticles; NM, nanomaterials.
150x101mm (300 x 300 DPI)

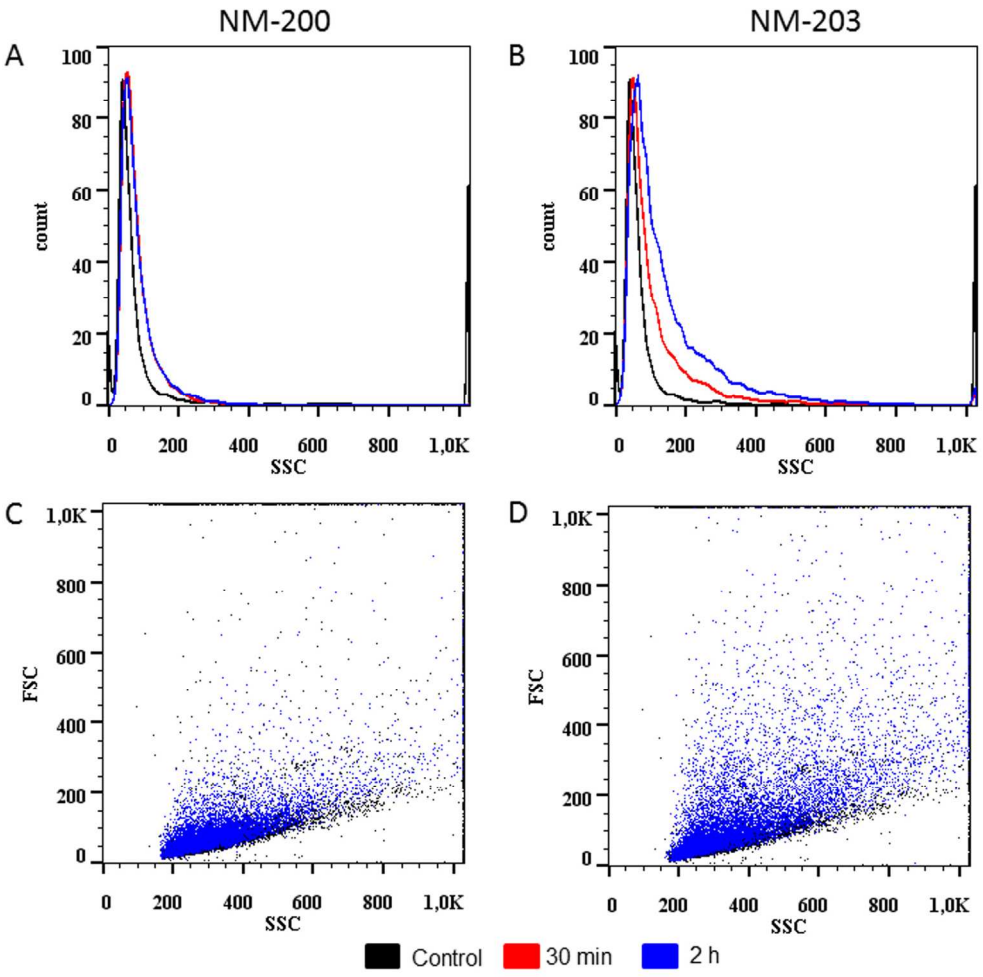

FIG. 3. Internalization of ASNP into RAW264.7 cells. Cells, grown for 24 h in complete growth medium, were treated with 5 μg/cm^2 of NM-200 (A-C) and NM-203 (B-D). After 30 min or 2 h of treatment, SSC was analyzed using FC500™ flow cytometer (see Materials and Methods). Histograms of cells treated for 30 min (red) or 2 h (blue), A, B. Representative cytograms at 2 h (C, D). Black dots, control, untreated cells. Abbreviations: SSC, side scatter.
150x146mm (300 x 300 DPI)

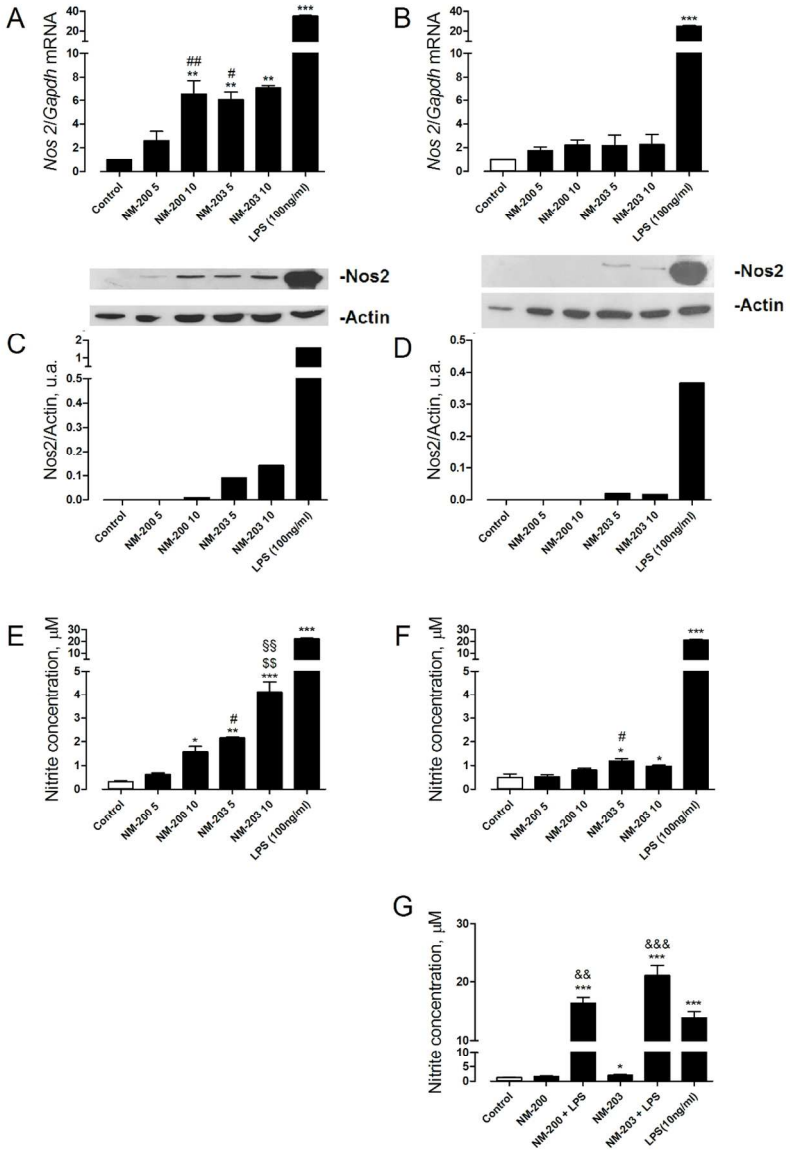

FIG. 4. Effects of NM-200 and NM-203 on Nos2 expression and NO production in MH-S and RAW264.7 cells. For (A), (B), (C), (D), (E) and (F), cells, MH-S and RAW264.7 cells, grown for 24h in complete growth medium, were treated with 5 or 10 µg/cm^2 of NM-200 and NM-203, or with LPS (100 ng/ml), used as a positive control. (A-B) After 24 h of treatment, mRNA was extracted and the expression of *Nos2* evaluated as described in Materials and Methods. (C-D) The expression of the protein Nos2 was assessed through Western Blot in cultures treated in parallel and extracted after 48 h of treatment. A representative blot is shown, with actin used for loading control (upper panel). In the lower panel the densitometric analysis of the same blot is shown. The experiment was performed twice with comparable results. (E-F) Nitrite concentration was determined in the culture medium of the cells used for the experiment shown in (C-D). For (G), RAW264.7 were treated with 10 µg/cm^2 of NM-200 or NM-203 in the absence or in the presence of LPS (10 ng/ml). After 48 h of treatment, nitrite concentration was determined in the culture medium. For (A) and (B), data are means ± S.D. of 2 independent determinations, each performed twice. For (E) and (F), data are means of four independent determinations ± S.D. For (G), data are means ± S.D. of 3 independent

determinations. *p<0.05, **p<0.01 and ***p<0.001 *vs.* untreated, control cells. #p<0.05 and ##p<0.01 *vs.* 5 µg/cm^2 of NM-200. $$p<0.01 *vs.* 10 µg/cm^2 of NM-200. §§p<0.01 *vs.* 5 µg/cm^2 of NM-203. ££p<0.01 and £££p<0.001 vs. LPS. Abbreviations: ASNP, amorphous silica nanoparticles; A.U., arbitrary units; *Gapdh*, Glyceraldehyde 3-phosphate dehydrogenase (gene); LPS, lipopolysaccharide; NM, nanomaterials; Nos2, inducible nitric oxide synthetase; S.D., standard deviation.
99x146mm (300 x 300 DPI)

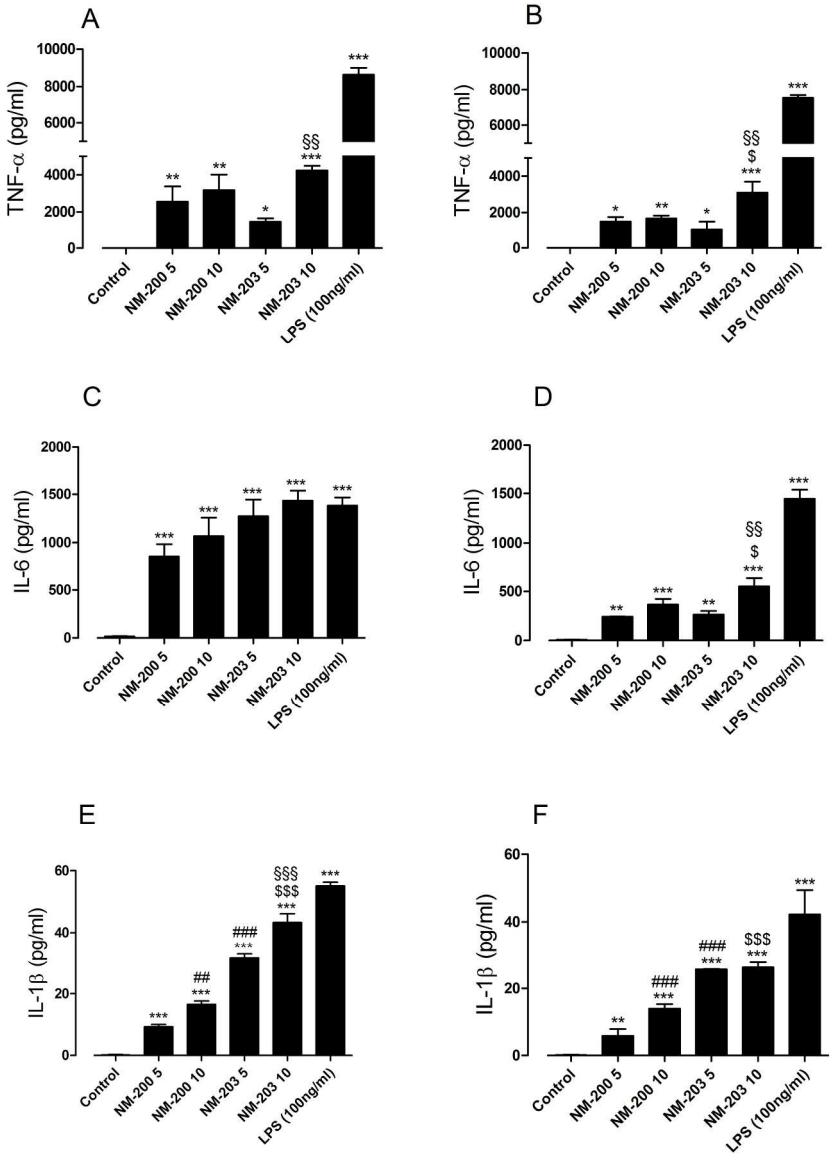

FIG. 5. TNF-α, IL-6 and IL-1β secretion in MH-S and RAW264.7 cells. Cells, grown for 24 h in complete growth medium, were treated with 5 or 10 μg/cm^2 of NM-200 or NM-203 or with LPS (100 ng/ml), as a positive control. After 6, 12 or 48 h of treatment, for TNF-α, IL-6 or IL-1β respectively, the indicated cytokines were measured in the extracellular medium, as described under Materials and Methods. (A), (C) and (E): MH-S; (B), (D), and (F): RAW264.7. Data are means of 3 independent determinations ± S.D. **p<0.01 and ***p<0.001 *vs.* untreated, control cells; ##p<0.01 and ###p<0.001 *vs.* 5 μg/cm^2 of NM-200. $p<0.05, $$p<0.01 and $$$p<0.001 *vs.* 10 μg/cm^2 of NM-200. §§p<0.01 and §§§p<0.001 *vs.* 5 μg/cm^2 of NM-203. Abbreviations: IL-1β, interleukin-1beta; IL-6, interleukin-6; LPS, lipopolysaccharide; NM, nanomaterials; S.D., standard deviation; TNF-α, tumor necrosis factor alpha.
203x275mm (300 x 300 DPI)

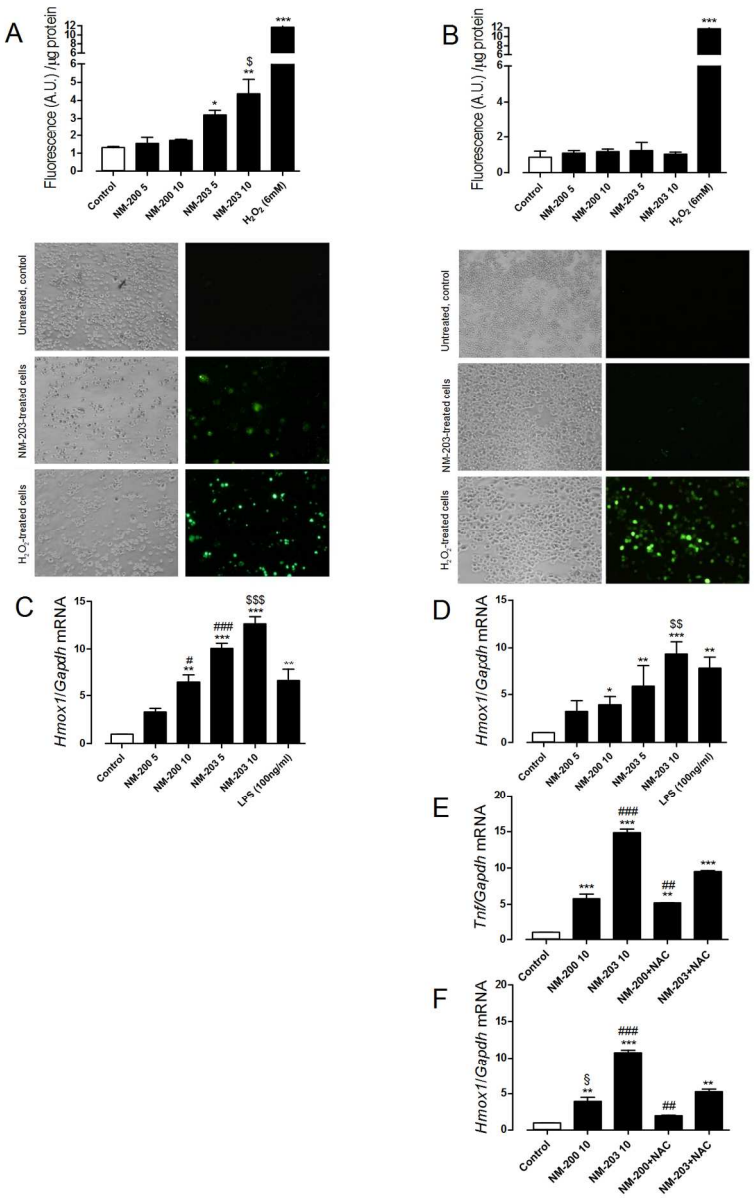

FIG. 6. ROS production, *Hmox1* and *Tnf* induction in macrophages. For (A), (B), (C), (D), cells, grown in complete growth medium, were treated with 5 or 10 µg/cm^2 of NM-200 or NM-203 or with H_2O_2 (6 mM), as a positive control. (A) and (B). After 24 h of treatment, MH-S (A) or RAW264.7 cells (B) were incubated for 2 h with CM-H_2DCF-DA (5 µM). Fluorescence was determined as described under Materials and Methods. Data are means ± S.D. of 3 independent determinations, each performed twice, *p<0.05, **p<0.01 and ***p<0.001 *vs.* untreated, control cells; $p<0.05 *vs.* 10 µg/cm^2 of NM-200. Before the determination of cell CM-H_2DCF-DA, images of representative fields were taken in phase contrast or with fluorescence microscope. x100. (C) and (D). After 6 h of treatment with ASNP or LPS (100 ng/ml, positive control), mRNA was extracted and the expression of *Hmox1* evaluated as described in Materials and Methods. (C), MH-S; (D), RAW264.7. Data are means ± S.D. of 2 independent determinations, each performed twice. *p<0.05, **p<0.01 and ***p<0.001 *vs.* untreated, control cells; #p<0.05 and ###p<0.001 *vs.* 5 µg/cm^2 of NM-200; $$p<0.01 and $$$p<0.001 *vs.* 10 µg/cm^2 of NM-200. (E) and (F), RAW264.7 cells were treated for 8 h with 10 µg/cm^2 of NM-200 or NM-203. As indicated, NAC (1 mM) was added 1 h before the

incubation with ASNP and maintained throughout the experiment. At the end of the incubation, mRNA was extracted, and the expression of *Tnf* (E) and *Hmox1* (F) was evaluated as described in Materials and Methods. Data are means ± S.D. of 3 independent determinations. **p<0.01 and ***p<0.001 *vs.* untreated, control cells; ##p<0.01 and ###p<0.001 *vs.* NM-203+NAC; §p<0.05 *vs.* NM-200+NAC. Abbreviations: ASNP, amorphous silica nanoparticles; A.U., arbitrary units; CM-H_2DCF-DA,5-(and-6)-chloromethyl-2',7' dichlorodihydrofluorescein diacetate, acetyl ester; *Hmox1*, Hemeoxygenase 1 (gene); H_2O_2, oxygen peroxyde; LPS, lipopolysaccharide; NAC, N-acetyl-cysteine; NM, nanomaterials; S.D., standard deviation; *Tnf*, tumor necrosis factor-alpha (gene).
150x233mm (300 x 300 DPI)